

PHOSPHOTRIESTERASE: AN ENZYME IN SEARCH OF ITS NATURAL SUBSTRATE

By FRANK M. RAUSHEL, *Department of Chemistry, Texas A&M University, College Station, Texas 77843* and HAZEL M. HOLDEN, *Department of Biochemistry, University of Wisconsin, Madison, Wisconsin 53706*

CONTENTS

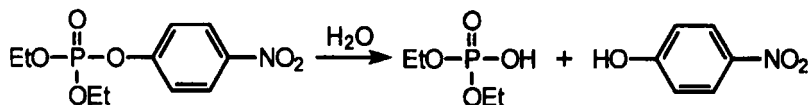
- I. Introduction
- II. Structure
 - A. Protein Sequence
 - B. Active Site Residues
 - C. Reconstitution of Apo-Enzyme
 - D. ¹¹³Cd-NMR Spectroscopy
 - E. EPR Spectroscopy
 - F. Mutagenesis of Active Site Residues
 - G. Structure of the Apo-Form of Phosphotriesterase
 - H. Structure of the Cd²⁺/Cd²⁺-Substituted Enzyme
 - I. Structure of the Zn²⁺/Zn²⁺-Containing Enzyme
 - J. Comparison with Other Enzymes
 - K. Modifications to Carbamylated Lysine
- III. Mechanism of Action
 - A. Stereochemistry at Phosphorus Center
 - B. Determination of Rate-Limiting Steps
 - C. Effects of Solvent Viscosity
 - D. pH-Rate Profiles
 - E. The Role of Binuclear Metal Center
 - F. Heavy Atom Isotope Effects
 - G. Mechanism-Based Inhibitors
 - H. Mechanism of Action
- IV. Substrate Specificity
 - A. Alterations to Substrate Specificity
- V. Summary
- Acknowledgments
- References

I. Introduction

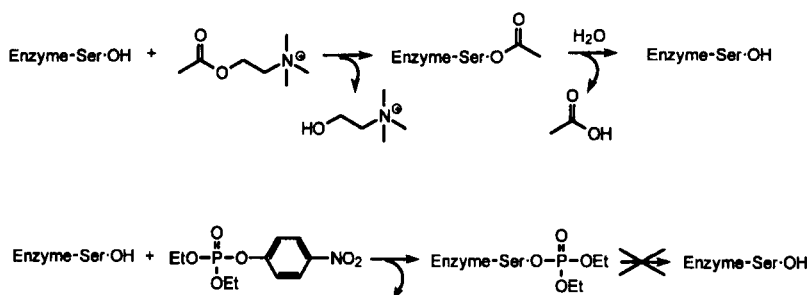
Approximately 25 years ago two strains of unrelated soil bacteria (*Pseudomonas diminuta* and *Flavobacterium* sp.) were isolated that had the ability to hydrolyze, and thus detoxify, a broad range of organophosphate insecticides and military-type nerve agents (Munnecke, 1976). The specific chemical reaction catalyzed by these bacterial strains, as exemplified with the insecticide paraoxon, is shown in Scheme 1. This enzymatic transformation is rather interesting since there are very few, if any, naturally occurring organophosphate triesters that have been isolated and characterized. Moreover, a protein that is capable of hydrolyzing organophosphates may eventually find commercial applications for the detoxification of agricultural insecticides and chemical warfare nerve agents.

Organophosphate triesters and related phosphonate diesters are extremely toxic because of their ability to specifically inactivate the enzyme acetylcholinesterase (AChE). Upon incubation of AChE with activated organophosphates, the enzyme rapidly forms a phosphoenzyme intermediate with an active site serine residue. This intermediate cannot be further processed by AChE at a significant rate and thus the catalytic function of the enzyme is destroyed. Since AChE is critical for nerve function, via the hydrolysis of acetylcholine, this inactivation event is lethal to a variety of cell types. The reactions catalyzed by AChE with acetylcholine and paraoxon are summarized in Scheme 2.

The bacterial phosphotriesterase (PTE) treats this class of organophosphate nerve agents not as potent inactivators of enzyme function, but rather as very good substrates with extraordinary turnover numbers. Since organophosphate triesters were not widely released into the environment as agricultural pesticides prior to World War II, it has been difficult to understand how the catalytic activities discovered for PTE could have rapidly evolved during this very short time interval. If PTE has not evolved to specifically hydrolyze organophosphate nerve agents, then the protein must catalyze another metabolic function that has not been discovered. The complete gene sequence for this enzyme has provided no substantive clues as to the



Scheme 1



metabolic role of this enzyme. At the time of discovery, there were no known protein sequences that were homologous to PTE. However, this situation has been clarified somewhat in the intervening period (Holm and Sander, 1997).

Our goal for this review is to provide a detailed account of the relationship between structure, function, and mechanism of this fascinating enzyme and then attempt to correlate the mechanism and structure of this protein with related examples of a growing superfamily of hydrolase enzymes.

II. Structure

A. PROTEIN SEQUENCE

The gene for the bacterial PTE has been sequenced from *P. diminuta* and *Flavobacterium* sp. (Mulbry and Karns, 1989; Serdar et al., 1989). The genes for PTE from both organisms are found within extra chromosomal plasmids. Surprisingly, the DNA sequences are identical, and in both cases the protein is translated as a larger precursor protein prior to the cleavage of a 29-amino acid leader peptide from the N-terminal end of the proenzyme to form the mature enzyme (Mulbry and Karns, 1989). The complete sequence of the unprocessed protein is presented in Figure 1. The constitutively expressed proteins in the native organisms are found as membrane-associated complexes (Brown, 1980; McDaniel, 1985).

The gene for the bacterial PTE has been subcloned into a variety of expression vectors (McDaniel, 1985) and the protein purified to homogeneity using insect cells (Dumas et al., 1989a; Dumas and Raushel, 1990a), *Streptomyces lividans* (Rowland et al., 1991), and *Escherichia coli* (Serdar et al.,

1	MQTRRVVLKS	AAAAGTLLGG	LAGCASVAGS	IGTGDRINTV	RGFITISEAG	50
51	FTLTHEHICG	SSAGFLRAWP	EFFGSRKALA	EKAVRGLRRA	RAAGVRTIVD	100
101	VSTFDIGRDV	SLLAEVSRAA	DVEHVAATGL	WFDPPLSMRL	RSVEELTQFF	150
151	LREIQYGIED	TGIRAGIIKV	ATTGKATPFQ	ELVLKAAARA	SLATGVFVTT	200
201	HTAASQRDGE	QQAIFESSEG	LSPSRVCIGH	SDDTDDLSTL	TALAARGYLI	250
251	GLDHIPHSAI	GLEDNASASA	LLGIRSWQTR	ALLIKALIDQ	GYMKQILVSN	300
301	DWLFQFSSYV	TNIMDVMDRV	NPDGMAFIPL	RVIPFLREKG	VPQETLAGIT	350
351	VTNPARFLSP	TLRAS				

Figure 1. Amino acid sequence for the bacterial phosphotriesterase from *Pseudomonas diminuta*.

1989). Significant improvements in the levels of protein expression have been obtained by deletion of the DNA encoding the 29-amino acid leader sequence (Mulbry and Karns, 1989; Serdar et al., 1989).

B. ACTIVE SITE RESIDUES

In order to catalyze the hydrolysis of an organophosphate triester, an enzyme must function to activate the hydrolytic water molecule for nucleophilic attack and enhance the electrophilic properties of the phosphorus center. Initial speculation on the chemical mechanism of PTE suggested that the hydrolytic water molecule could be activated by general base catalysis and that the leaving group of the organophosphate triester could be activated by general acid catalysis (Donarski et al., 1989; Dumas and Raushel, 1990b). This particular aspect of the reaction mechanism and active site structure was first examined for the purified enzyme via the determination of the pH-rate profile. When paraoxon is used as the substrate, the pH profile versus k_{cat} with PTE is as shown in Figure 2. There is a plateau of catalytic activity above pH ~7 and a loss of activity below pH ~6.5. A fit of the experimental data to the appropriate equation gave a pK_a for a single ionizable group of 6.1 (Dumas and Raushel, 1990b). A similar profile was found for k_{cat}/K_m . Since the substrate cannot lose protons within the pH range examined, it thus appeared that a single group at the active site of PTE must be ionized for maximum catalytic activity. The pH-rate profile was thus consistent with a residue that served to activate the hydrolytic water molecule via general base catalysis. Since there was no loss of activity at high pH there was no evidence for general acid catalysis during the departure of the leaving group phenol. This outcome was not entirely unexpected since the

pK_a of *p*-nitrophenol is approximately 7.0 and there is little to be gained by stabilization of the leaving group phenol. In an effort to determine the identity of the active site residue responsible for the single ionization that was found in the pH-rate profile, the effect of temperature on the pK_a value was measured. The ΔH_{ion} was determined to be 7.9 kcal/mol (Dumas and Raushel, 1990b). The effect of organic solvents indicated that the group was a cationic acid. These data were most consistent with the ionization of a single histidine residue at the active site of PTE.

Confirmation of this assignment was sought through the utilization of group-specific reagents. No significant inactivation could be obtained upon incubation of the enzyme with dithionitrobenzoic acid (DTNB), carbodiimide, pyridoxal, butanedione, or iodoacetate (Dumas and Raushel, 1990b). These results appeared to eliminate cysteine, lysine, arginine, aspartate, and glutamate as accessible residues within the active site. However, the enzyme could be quantitatively inactivated with the histidine-specific reagent diethylpyrocarbonate (DEPC) and the metal chelator, *o*-phenanthroline. Analy-

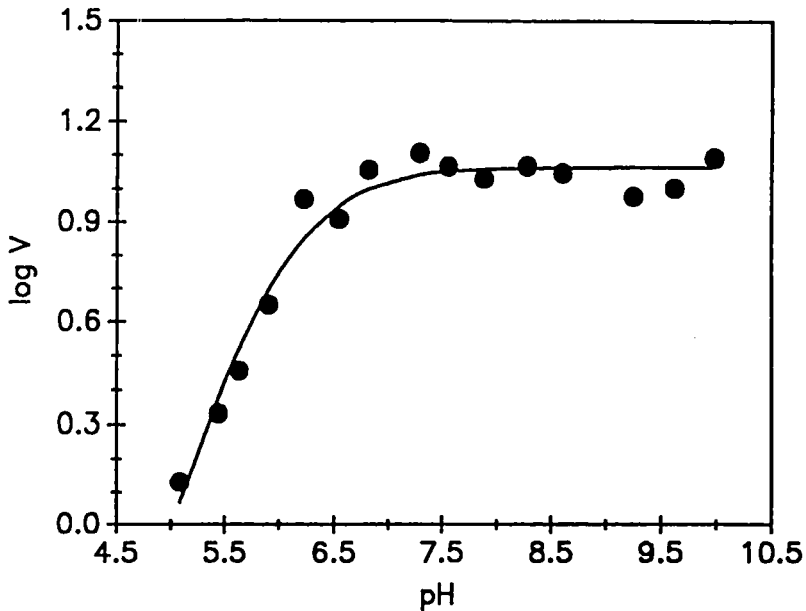


Figure 2. pH-rate profile for the hydrolysis of paraoxon as catalyzed by the bacterial phosphotriesterase.

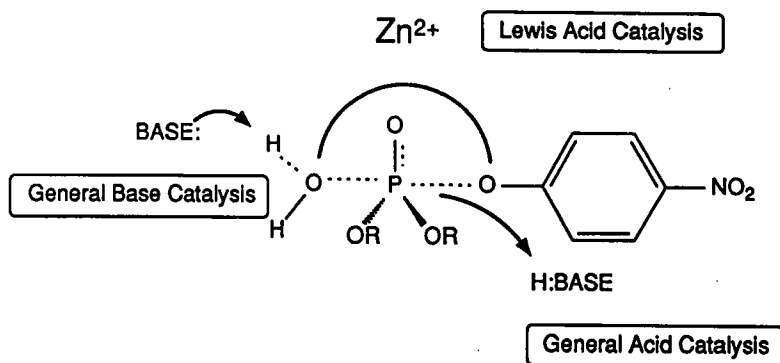


Figure 3. Initial model for the mechanism of organophosphate hydrolysis by phosphotriesterase.

sis of the DEPC inactivation kinetics as a function of pH was consistent with a pK_a value of 6.1 for the histidine that was labeled under the experimental conditions (Dumas and Raushel, 1990b). No loss of activity was observed in the presence of substrate analogs and thus the labeled histidine appeared to be within the active site. Atomic absorption spectroscopy confirmed the presence of zinc bound to the protein. Based upon these results a working catalytic mechanism was proposed as illustrated in Figure 3. In this mechanism the function of the ionized histidine is to remove a proton from the metal-bound water molecule. In addition to serving as a template for the hydrolytic water molecule, the lone zinc ion could serve to polarize the phosphoryl oxygen bond and thus make the phosphorus center more electrophilic.

C. RECONSTITUTION OF APO-ENZYME

The initial discovery that the bacterial phosphotriesterase contained bound zinc prompted a series of experiments designed to substitute other divalent cations into the enzyme active site (Omburo et al., 1992). The most successful of these experiments involved the utilization of a metal chelator to make apo-enzyme and then reconstitution of the metal-free enzyme with a variety of divalent cations. Metal chelators such as *o*-phenanthroline were found to be far more efficient at the removal of bound-metal from the protein than ethylenediaminetetraacetic acid (EDTA). Thus, the second-order rate constant for the inactivation of PTE by *o*-phenanthroline and EDTA are $1.6 \text{ M}^{-1} \text{ s}^{-1}$ and $8 \times 10^{-4} \text{ M}^{-1} \text{ s}^{-1}$, respectively (Omburo et al., 1992). The apo-enzyme has less than 1% of the catalytic activity exhibited by the wild-type enzyme. The apo-

enzyme was stable when frozen at -78°C for a period of at least six months and full enzymatic activity could be recovered upon the addition of zinc.

Reconstitution of the apo-enzyme with a variety of divalent cations revealed two very interesting structural and mechanistic features about PTE. Shown in Figure 4 is a plot of the recovered enzymatic activity as a function of metal ion added per equivalent of apo-enzyme. Remarkably, the protein could be reconstituted with Co^{2+} , Cd^{2+} , and Zn^{2+} . The Co^{2+} - and Cd^{2+} -substituted proteins were even more active than the Zn^{2+} -substituted protein. For each of the divalent cations added to the system there was a linear increase in the catalytic activity until the ratio of two metal ions per protein equivalent was achieved. Thus, PTE requires two metal ions for full catalytic activity rather than the single metal ion as originally believed (Omburo et al., 1992). Additional experiments (not shown) demonstrated that Mn^{2+} and Ni^{2+} were also able to activate the enzyme. The optimum pH for reconstitution of apo-enzyme was found to be pH 7–8.5. A summary of the catalytic constants by each of the

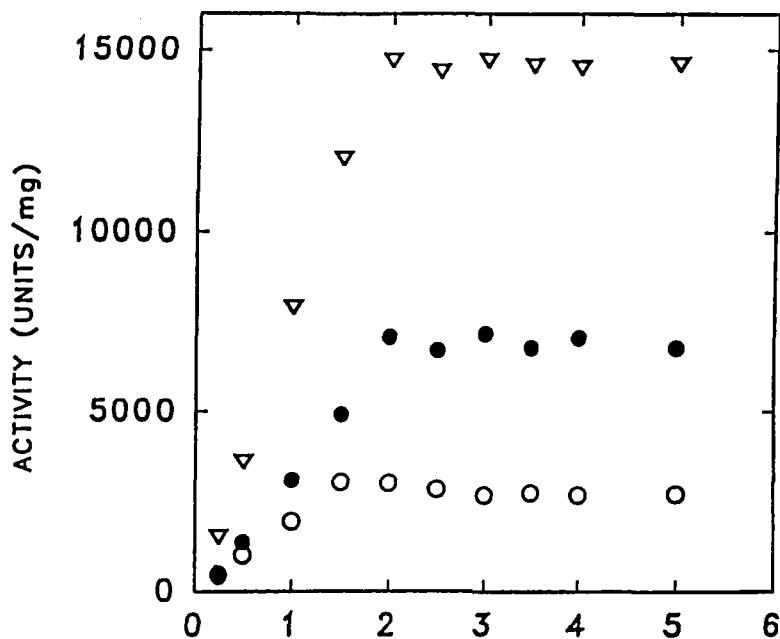


Figure 4. Reconstitution of the apo-phosphotriesterase with various amounts of Co^{2+} , Zn^{2+} , and Cd^{2+} .

TABLE 1
Kinetic Constants for Metal Substituted Phosphotriesterase^a

Metal	K_m (μM)	k_{cat} (s^{-1})	k_{cat}/K_m ($10^7 \text{ M}^{-1} \text{ s}^{-1}$)
Zn ²⁺	90	2400	2.7
Co ²⁺	200	7800	4.0
Mn ²⁺	80	1800	2.2
Cd ²⁺	400	4600	1.2
Ni ²⁺	150	6000	3.9

^aDetermined for paraoxon at pH 9.0.

metal-substituted forms of PTE for the hydrolysis of paraoxon is presented in Table 1. Unfortunately, the titration of apo-enzyme with the various divalent cations provided no clues with regard to whether one or both metal ions were required for catalytic activity. Moreover, it could not be determined whether these metal ions were required for structural or catalytic functions.

D. ¹¹³Cd-NMR SPECTROSCOPY

The environment of the metal ion binding site(s) was initially probed with nuclear magnetic resonance (NMR) spectroscopy (Omburo et al., 1993). Cadmium has two isotopes that are NMR active, ¹¹³Cd²⁺ and ¹¹¹Cd²⁺. Prior investigations with model systems and metal binding sites in proteins of known structure had clearly demonstrated that a great deal of information could be obtained about the direct ligands to each of these metals from a determination of the chemical shift (Summers, 1988). In model systems the chemical shift range for ¹¹³Cd²⁺ extends in excess of 900 ppm. The most downfield signals are observed for complexes that are composed of all thiolate ligands from cysteine while the most upfield signals are those for complexes with all-oxygen bearing ligands from water or carboxylates (aspartate or glutamate). Nitrogen ligand sets are intermediate in chemical shift between the sulfur and oxygen ligands.

The ¹¹³Cd²⁺ spectrum of PTE containing two Cd²⁺ per monomeric protein is presented in Figure 5A. The spectrum clearly shows that each of the metal ions is in a slightly different chemical environment. The observed chemical shifts are 116 and 212 ppm. The chemical shift position excluded ligation by even a single cysteine group and strongly suggested that the ligand set consisted of a mixture of oxygen (water, carboxylate) and nitrogen (histidine) ligands. The more downfield signal was expected to arise from Cd²⁺, which

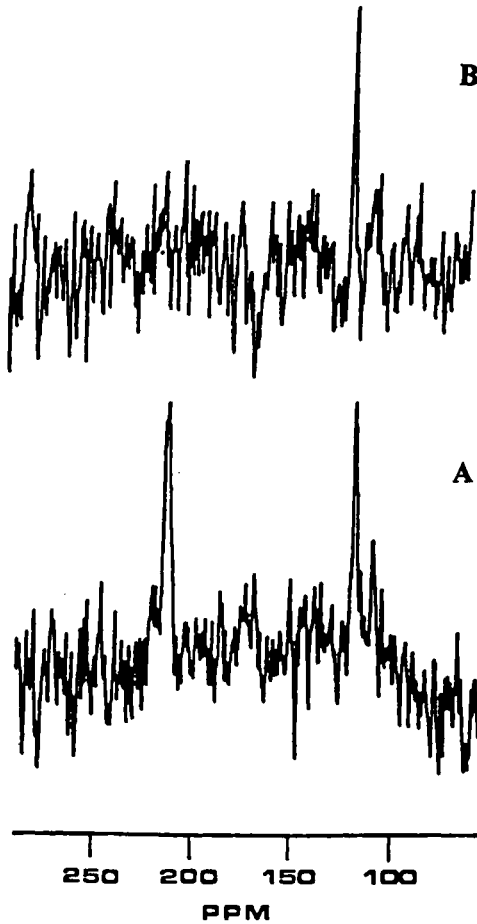


Figure 5. ^{113}Cd -NMR spectra of bacterial phosphotriesterase. (A) Apo-enzyme reconstituted with 2 equivalents of Cd^{2+} . (B) Apo-enzyme reconstituted with one equivalent each of Zn^{2+} and Cd^{2+} .

had a higher percentage of nitrogen ligands than the more upfield signal. The best estimates, made at that time, proposed that the cadmium with the more downfield signal was bound to three nitrogen ligands and one oxygen ligand while the cadmium exhibiting the upfield signal was bound to two nitrogen ligands and two oxygen ligands. This analysis assumed that the environment for each metal ion was tetrahedral. These conclusions were not

entirely correct, as later discovered by the solution of the X-ray crystal structure for PTE. Nevertheless, these studies clearly demonstrated that a majority of the ligands to each of these metal ions originated from the imidazole side chain of histidine residues (Omburo et al., 1993).

^{113}Cd -NMR spectroscopy provided further insight into the structure of an unusual hybrid of PTE. It was found that a hybrid containing one Cd^{2+} and one Zn^{2+} could be constructed (Omburo et al., 1993). The catalytic properties of the Cd/Zn-hybrid more closely resembled those of Zn/Zn-PTE rather than Cd/Cd-PTE, and thus one metal ion appears to dominate the catalytic properties. The ^{113}Cd -NMR spectrum of the hybrid is presented in Figure 5B. Only the single upfield resonance was observed and thus it appeared that cadmium was uniquely occupying only one of the two sites while zinc was located at the other site. This metal hybrid complex may be of great utility in defining the specific functions of the individual metals in binding and catalysis.

E. EPR SPECTROSCOPY

Since the divalent cations bound to PTE could be substituted with Mn^{2+} with high occupancy and relatively high catalytic activity, electron paramagnetic resonance (EPR) spectroscopy was utilized to provide additional information with regard to protein-metal and metal-metal interactions (Chae et al., 1993). The ^{113}Cd -NMR evidence provided no information about whether the protein contained two mononuclear metal centers or if a single binuclear metal center was operable. Shown in Figure 6 is the EPR spectrum of the $\text{Mn}^{2+}/\text{Mn}^{2+}$ -PTE at 10 K. The X-band EPR spectrum is quite complex. The predominant features were near $g=2$ and exhibited what appeared to be more than 26 Mn hyperfine splittings at ~ 45 gauss intervals. The large number of hyperfine splittings, separated by approximately half the magnitude expected for a mononuclear Mn^{2+} -center, suggested the presence of two spin-coupled Mn^{2+} ions. This conclusion was also supported by the Q-band spectrum obtained under similar experimental conditions (Chae et al., 1993). The temperature dependence of the X-band signals provided further evidence that the two manganese ions were antiferromagnetically coupled to one another (Chae et al., 1993). Similar spectra had previously been noted with arginase (Reczykowski and Ash, 1992), enolase (Poyner and Reed, 1992), concanavalin A (Antanaitis et al., 1987), and catalase (Khangulov et al., 1990). These data ruled out the existence of two independent mononuclear sites. Thus, the most likely structure was a coupled binuclear center with a bridging ligand of unknown identity (Chae et al., 1993, 1995). Taken

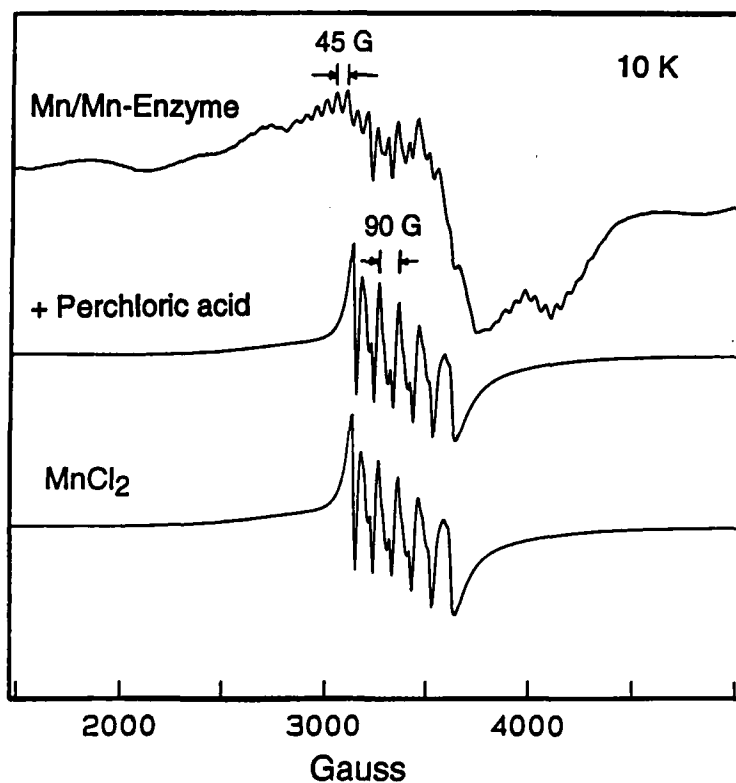


Figure 6. Electron paramagnetic resonance spectrum (X-band) of the apo-enzyme reconstituted with two equivalents of Mn^{2+} .

together the $^{113}Cd^{2+}$ -NMR studies and the Mn^{2+} -EPR investigations pointed to the existence of a binuclear metal center where a majority of the direct ligands to the metal ions originated with the imidazole side chains of histidine.

MUTAGENESIS OF ACTIVE SITE RESIDUES.

The spectroscopic and chemical labeling experiments implicated the essential nature of one or more histidine residues at the active site of the bacterial phosphotriesterase. These results prompted two independent investigations toward the identification of those histidine residues required for catalytic activity (Kuo and Rauschel, 1994; Lai et al., 1994). In PTE there

are only seven histidine residues in the entire molecule and each of these histidine residues was mutated to an asparagine residue. Of the seven residues only His-123 was without measurable effects on the catalytic activities after mutation to asparagine. The remaining six residues, His-55, His-57, His-201, His-230, His-254, and His-257, were all diminished in activity to some extent. Working models, constructed at that time, that attempted to assign individual histidine residues to specific metal ions within the binuclear metal cluster proved later to be slightly incorrect. However, the X-ray structure of PTE clearly demonstrated that His-123 was away from the active site and that the remaining six histidines were in the active site but that only His-55, His-57, His-201, and His-230 had coordinate bonds to either of the two metals (Benning et al., 1995). All of these histidine residues have also been mutated in a combinatorial library to cysteine (Watkins et al., 1997a)

G. STRUCTURE OF THE Apo-FORM OF PHOSPHOTRIESTERASE

The various structural analyses of phosphotriesterase that were initiated in the spring of 1994 can be aptly described as one surprise after another. Indeed, crystals of the Cd²⁺-substituted enzyme were first observed with polyethylene glycol 8000, 100 mM bicine (pH 9.0), and 1 M LiCl as the precipitant (Benning et al., 1994). As the X-ray model of phosphotriesterase was being built, however, it became obvious that there were no large peaks in the electron density map corresponding to the bound Cd²⁺ ions of the binuclear metal center and, in fact, the crystallization conditions employed had effectively removed the metals from the protein. While the structural determination of the apo-form of phosphotriesterase was unintentional, this analysis did provide the first three-dimensional glimpse of the enzyme. Indeed, from the packing arrangement of the molecules in the crystalline lattice, it was immediately obvious that, contrary to previous reports (Dumas et al., 1989a), the quaternary structure of the enzyme was dimeric rather than monomeric. Shown in Figure 7 is a ribbon representation of the phosphotriesterase dimer. The total surface area buried upon dimer formation is approximately 3200 Å² using a search probe radius of 1.4 Å. The subunit:subunit interface is formed primarily by two regions delineated by Ser-61 to Phe-73 and Met-138 to Phe-149. In particular, there are four aromatic residues, Phe-65, Trp-69, Phe-72, and Phe-73, that participate in various stacking interactions as indicated by the ball-and-stick representations in Figure 7. Apart from these aromatic contacts, there are numerous electro-

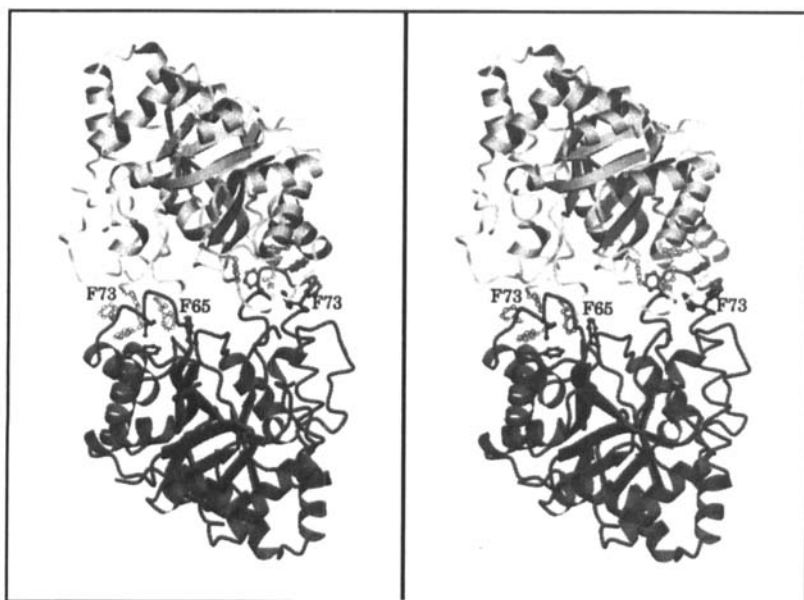


Figure 7. Ribbon representation of the phosphotriesterase dimer. Those amino acid residues forming a hydrophobic patch at the dimeric interface are displayed in ball-and-stick representations.

static interactions that also serve to stabilize the subunit:subunit interface of the dimer.

Each subunit of the dimer is roughly globular with overall dimensions of $51 \text{ \AA} \times 55 \text{ \AA} \times 51 \text{ \AA}$. As can be seen in Figure 7, the fold of each subunit is dominated by eight β -strands that wrap around to form a parallel β -barrel. This β -barrel is flanked on the outer surface by a total of 14 α -helices. In addition to the barrel motif, there are two antiparallel β -strands at the N-terminus. At the time of this investigation, amino acid sequence analyses failed to detect any similarity between phosphotriesterase and other proteins of known structure. Yet, this α/β -barrel motif is a very commonly occurring tertiary structural element in enzymes and is typically referred to as a "TIM-barrel" (Farber and Petsko, 1990). In these TIM-barrel enzymes, the active sites are invariably located at the C-terminal portion of the β -barrel. A close-up view of this region in PTE is shown in Figure 8. As originally predicted from site-directed mutagenesis experiments, His-55, His-57, His-201, His-230, His-254, and His-257 are, indeed, clustered within this active site re-

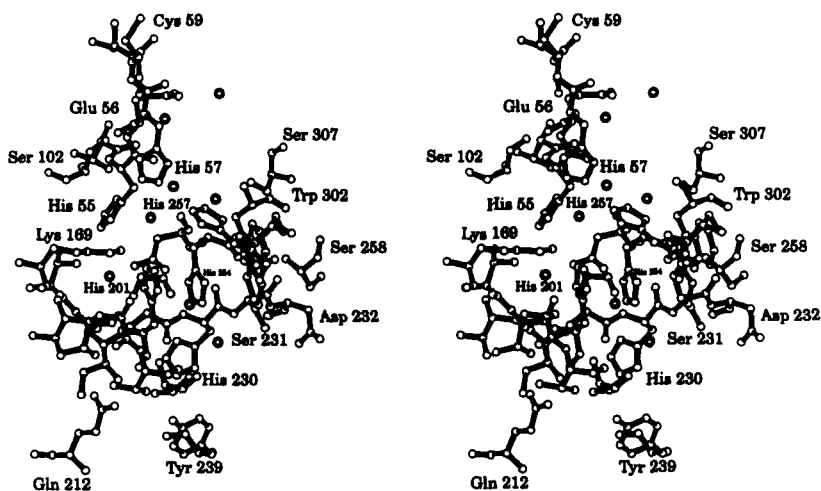


Figure 8. Close-up view near the C-terminal portion of the β -barrel. The *gray spheres* represent ordered solvent molecules.

gion (Kuo and Raushel, 1994; Lai et al., 1994). There is a striking stacking interaction between the imidazole rings of His-201 and His-254. In addition, there is a close contact between the ϵ -amino group of Lys-169 and $N^{\delta 1}$ of His-201 (2.1 Å). Even though this first structural analysis of phosphotriesterase was that of the apo-protein, nevertheless it resulted in the determination of the overall molecular motif of the enzyme, its active site location, and its proper quaternary structure.

H. STRUCTURE OF THE CD^{2+}/CD^{2+} -SUBSTITUTED ENZYME

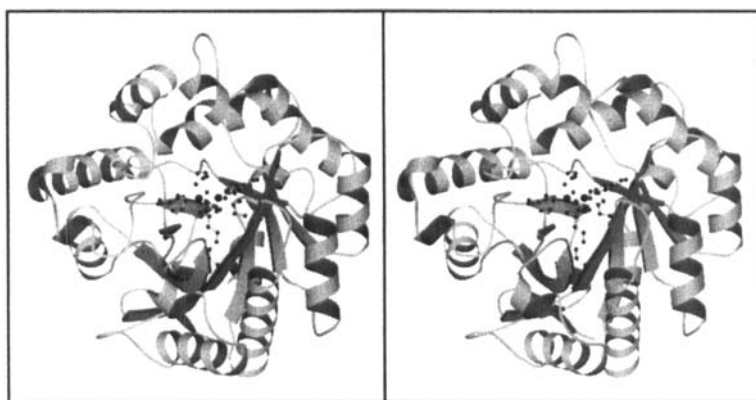
In an attempt to prepare samples of the native, metal-containing phosphotriesterase, the apo-enzyme crystals were subsequently transferred to various metal-containing solutions such as $CdCl_2$. Unfortunately the X-ray diffraction quality of the crystals deteriorated significantly such that it was not possible to collect X-ray data beyond 3.5 Å resolution. The next set of experiments involved crystallization of the cadmium-containing enzyme with polyethylene glycol but this time in the absence of lithium chloride and with the replacement of the buffer bicine with CHES. Again these experiments met with limited success until the substrate analog, diethyl 4-methylbenzylphosphonate, was added to the precipitant solution. Under these

conditions, crystals appeared within one week and diffracted to a nominal resolution of 2.0 Å. The structure of the holoenzyme was subsequently solved by the techniques of molecular replacement, solvent flattening, and molecular averaging (Benning et al., 1995).

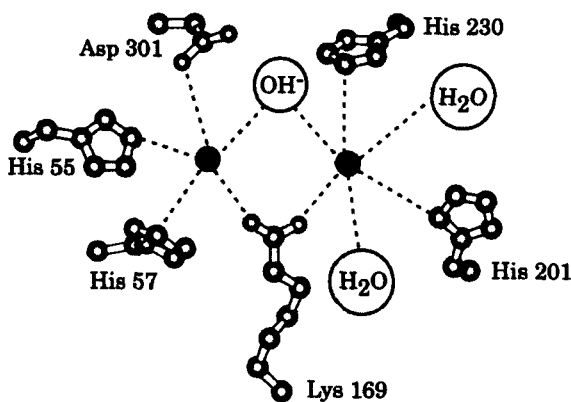
A ribbon representation of the Cd²⁺/Cd²⁺-containing PTE is displayed in Figure 9A. As predicted from the apo-enzyme structure, the binuclear metal center is, indeed, located at the C-terminal portion of the β-barrel. The substrate analog did not bind within this region, however, but rather at the interface between two symmetry-related molecules in the crystalline lattice. Quite unexpectedly, the bridging ligand for the binuclear metal center was not an aspartate, glutamate, or histidine residue but rather Lys-169, which, as indicated by the electron density, was carbamylated. Of the six histidine residues clustered at the end of the β-barrel, four are directly involved in metal ligation (His-55, His-57, His-201, and His-230). In addition, the carboxylate group of Asp-301 functions as a metal ligand.

A cartoon of the coordination geometry for the binuclear metal center is depicted in Figure 9B. The two cadmium ions are separated by 3.8 Å and are bridged by both the carbamylated lysine and a solvent molecule, most likely a hydroxide ion. The deeper buried cadmium ion is surrounded in a trigonal bipyramidal arrangement by His-55, His-57, Lys-169, Asp-301, and the bridging solvent. Lys-169, His-201, His-230, the bridging hydroxide ion, and two additional waters form a distorted octahedral arrangement around the more solvent-exposed cadmium. The metal:ligand bond lengths range from 2.1 Å to 2.7 Å.

Superpositions of the polypeptide chain backbones for the apo- and holoenzymes are given in Figure 10A. Even though these polypeptide chains are identical in amino acid sequence, they superimpose with a remarkable root-mean-square difference of 3.4 Å. The three-dimensional differences in these polypeptide chains are limited, however, to a few specific regions, the most striking of which occurs near Asp-301. In the apo-enzyme model, Asp-301 adopts dihedral angles of $\phi = -54.2^\circ$ and $\psi = -45.2^\circ$ while in the holoprotein, it assumes torsional angles of $\phi = 58.3^\circ$ and $\psi = 44.0^\circ$. This reversal from a right-handed to a left-handed helical conformation forces the polypeptide chains into completely different directions as can be seen in the close-up view presented in Figure 10B. A superposition of the active site regions for the apo- and holoenzyme models is depicted in Figure 11. In retrospect, it is not surprising that metal-soaking experiments with preformed apo-enzyme crystals met with limited success. As can be seen, apart from the position of His-57, there is a complete restructuring of the



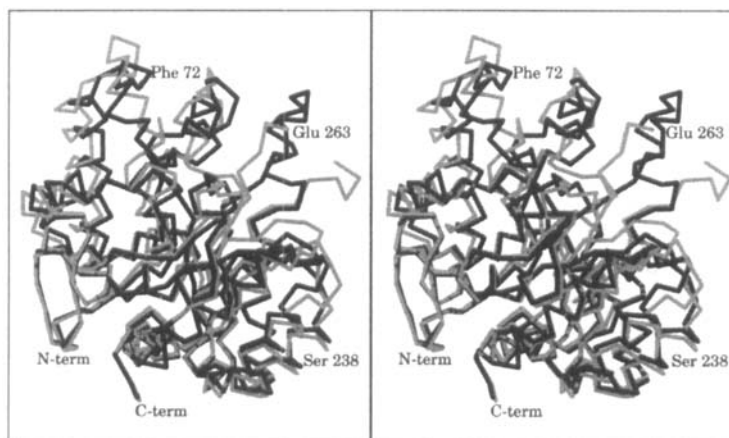
(a)



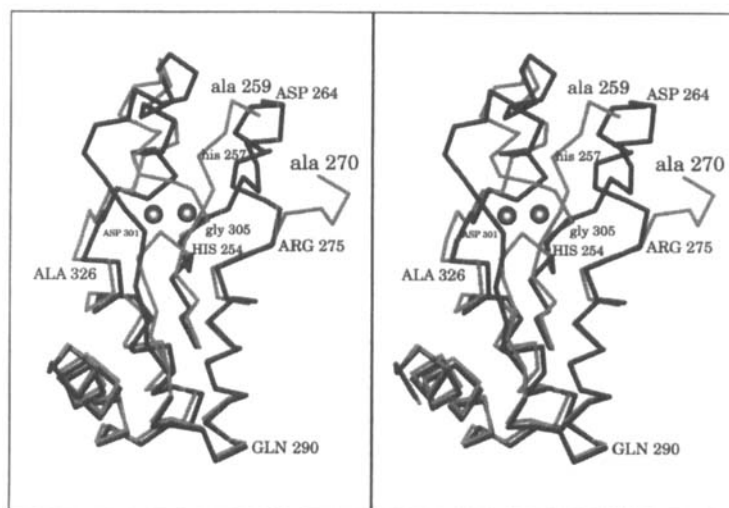
(b)

Figure 9. Structure of the $\text{Cd}^{2+}/\text{Cd}^{2+}$ -containing phosphotriesterase. A ribbon representation of one subunit is given in (a). Those residues involved in metal ligation are displayed as ball-and-sticks. A schematic of the coordination geometry about the binuclear metal center is displayed in (b).

amino acid side chains upon metal binding and, indeed, these dramatic differences clearly highlight the difficulties in predicting protein structures based simply upon amino acid sequences. In the case of phosphotriesterase, the three-dimensional architecture of the protein is dependent not only upon



(a)



(b)

Figure 10. Comparison of the apo- and holo-enzyme structures. α -Carbon traces for the apo- and holo-enzyme models are displayed in *gray* and *black*, respectively. The two structures differ most in the region shown in (b). Those amino acid residues indicated in lower- and upper-case refer to the apo- and holo-enzymes, respectively. The cadmium ions are represented by the *large spheres* near Asp 301.

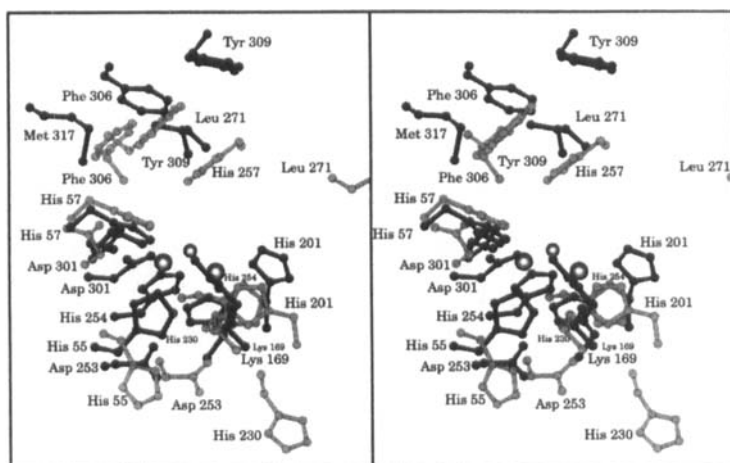


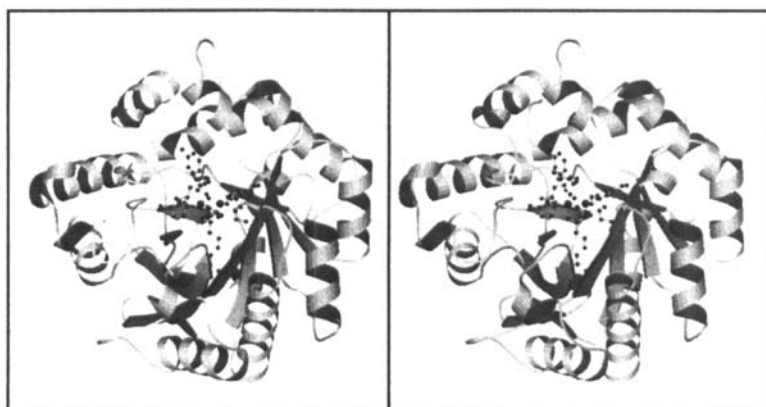
Figure 11. Superposition of the active site regions in the apo- and holo-enzyme models. The apo- and holo-forms of the enzyme are depicted in *gray* and *black*, respectively

its primary structure but also upon the presence or absence of the binuclear metal center.

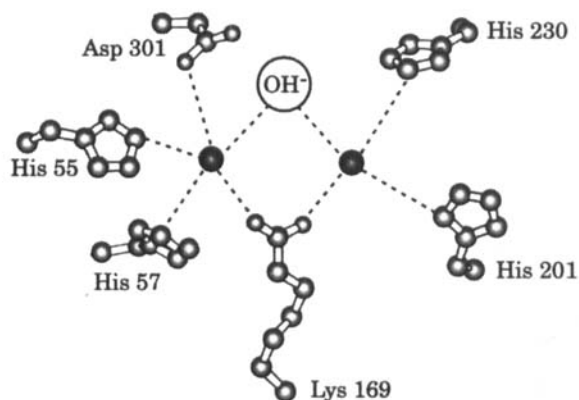
I. STRUCTURE OF THE Zn^{2+}/Zn^{2+} -CONTAINING ENZYME

While the molecular model of the Cd^{2+}/Cd^{2+} -substituted PTE was informative with regard to the overall fold of the holoenzyme and the coordination geometry of the binuclear metal center, the naturally occurring enzyme contains zinc. Consequently, the next goal in the structural analysis of PTE was to grow crystals of the Zn^{2+}/Zn^{2+} -containing enzyme. Again, crystals were obtained in the presence of the substrate analog, diethyl 4-methylbenzylphosphonate (Vanhook et al., 1996). This time the inhibitor not only bound within the hydrophobic pocket located between two monomers in the crystalline lattice, but also adjacent to the binuclear zinc center. Note that the α -carbon traces for the zinc- and cadmium-containing proteins superimpose with a root-mean-square deviation of 0.20 Å.

A ribbon representation of the Zn^{2+}/Zn^{2+} -containing enzyme with the bound inhibitor is depicted in Figure 12A and a cartoon of the coordination geometry for the binuclear metal center is displayed in Figure 12B. In the Zn^{2+}/Zn^{2+} -containing protein, the metals are separated by 3.3 Å and the zinc:ligand bond lengths range from 1.8 Å to 2.3 Å. Again, the deeper



(a)



(b)

Figure 12. Structure of the Zn^{2+}/Zn^{2+} -containing phosphotriesterase. A ribbon representation of one subunit is given in (A) and a cartoon of the coordination geometry is shown in (B).

buried metal ion is coordinated to the protein via the side chain functional groups of His-55, His-57, Lys-169, Asp-301, and the bridging solvent in a virtually identical trigonal bipyramidal arrangement as observed for the cadmium-substituted enzyme. The coordination geometry around the more sol-

vent-exposed zinc, however, has changed from octahedral to tetrahedral with the simple removal of water molecules from the coordination sphere. While the atomic radii for Zn^{2+} and Cd^{2+} are 0.74 Å and 0.97 Å, respectively, it appears that the polypeptide chain backbone of phosphotriesterase is ideally suited for accommodating such differences. Indeed, the protein atoms for these two forms of PTE, including side chains, superimpose with a root-mean-square deviation of 0.40 Å.

Perhaps the most notable aspect of the PTE active site is the lack of hydrogen bonding interactions between the protein and the inhibitor. A close-up view of the binding pocket is given in Figure 13. There is only one direct electrostatic interaction between the inhibitor and the protein. Specifically, the phosphoryl oxygen of the substrate analog is located 3.3 Å from $N^{\delta 1}$ of Trp-131 and 3.2 Å from $N^{\delta 1}$ of His-201. In addition, this oxygen is situated within 3.5 Å of the more solvent accessible zinc ion. The methylbenzyl group, as displayed in Figure 13, is wedged into a fairly hydrophobic pocket formed by His-257, Leu-271, Phe-306, and Met-317. Each of the two enantiotopic ethoxy groups of the inhibitor occupy quite distinct chemical environments. The *pro-R* ethoxy group is pointed toward Ile-106, Trp-131,

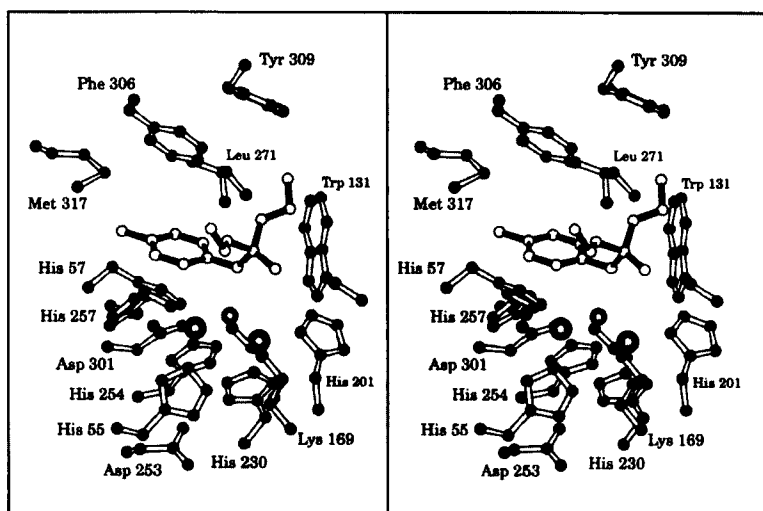


Figure 13. Close-up view of the region surrounding the bound inhibitor diethyl 4-methylbenzyl phosphonate. The protein model is depicted in *open bonds* while the inhibitor is displayed in *filled bonds*.

Leu-303, Phe-306, and Ser-308 while the *pro-S* moiety is directed away from the binuclear metal center toward the solvent and surrounded by Trp-131, Phe-132, Leu-271, Phe-306, and Tyr-309.

J. COMPARISON WITH OTHER ENZYMES

The employment of a binuclear metal center for catalytic activity is, by no means, limited to PTE. Binuclear metal centers are quite common and have been observed, for example, in bovine lens leucine aminopeptidase (Sträter and Lipscomb, 1995), kidney bean purple acid phosphatase (Sträter et al., 1995), *E. coli* alkaline phosphatase (Kim and Wyckoff, 1991), human inositol monophosphatase (Pollack et al., 1994), mammalian protein phosphatase-1 (Goldberg et al., 1995), *Bacillus cereus* phospholipase C (Hough et al., 1989), *E. coli* DNA polymerase I (Beese and Steitz, 1991), *Penicillium citrinum* P1 nuclease (Volbeda et al., 1991), among others. An elegant review of these enzymes can be found in Wilcox (1996). In these above-mentioned enzymes, the two metals are typically bridged by either solvent molecules, aspartate and glutamate residues, or both.

Thus far, the only other example of an enzyme that employs a carbamylated lysine as a bridging ligand is urease. This enzyme catalyzes the hydrolysis of urea and employs a binuclear nickel center for activity. Recent X-ray structural analyses of urease from *Klebsiella aerogenes* (Jabri et al., 1995) confirmed the participation of a carbamylated lysine residue in the formation of the binuclear metal center (Park and Hausinger, 1995). As can be seen in the superposition presented in Figure 14, the binuclear metal centers in PTE and urease are remarkably similar. As observed for PTE, the polypeptide chain of one domain of urease folds into a TIM-barrel. Likewise, in urease, the nickels are separated by a comparable distance of 3.5 Å. The more buried nickel ion in urease is surrounded by His-134, His-136, Asp-360, the bridging carbamylated Lys-217, and a hydroxide ion in a distorted trigonal bipyramidal arrangement. The second nickel is ligated to the protein via His-246, His-272, and the bridging lysine residue. Other than the similarities in their overall tertiary structures and the immediate environments surrounding the metal ions, however, the chemical nature of the active sites for PTE and urease are quite different.

Following the three-dimensional analyses of urease and PTE, Scanlan and Reid (1995) demonstrated that a portion of the nucleic acid sequence of the *E. coli* chromosome encodes a protein with 28% amino acid sequence identity to PTE. The three-dimensional structure of this protein, referred to as

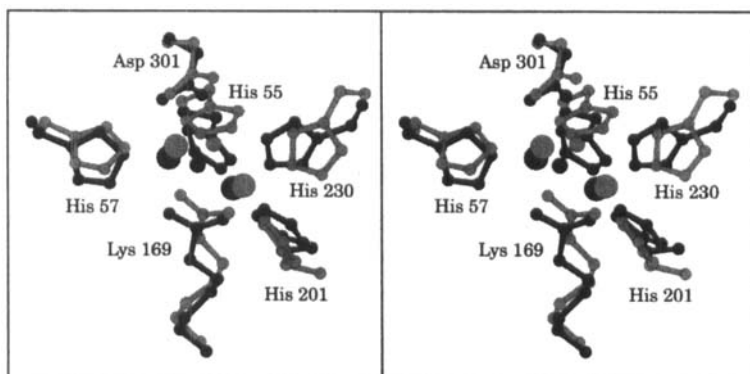


Figure 14. Superposition of the metal binding regions for the Zn^{2+}/Zn^{2+} -containing phosphotriesterase (PTE) and for urease. The PTE model is shown in *black* and the urease model is depicted in *gray*.

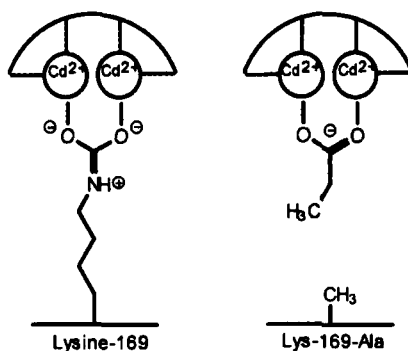
PHP (phosphotriesterase homology protein), was subsequently determined in the Fletterick laboratory to 1.7 Å resolution (Buchbinder et al., 1998) and, as expected, the fold is very similar to PTE. The two zinc ions observed binding to PHP are separated by 3.4 Å but in this case the bridging ligand is a glutamate (Glu-125) rather than a carbamylated lysine. As observed in urease and PTE, the deeper buried metal is again surrounded in a trigonal bipyramidal arrangement, specifically by His-12, His-14, Glu-125, Asp-243, and a molecule of unknown identity. The other zinc ion is ligated to PHP in a tetrahedral coordination sphere formed by His-158, His-186, Glu-125, and the unknown solvent molecule. The physiological function of PHP is presently unknown.

On the basis of both amino acid sequence analyses and the structural homologies between urease, PTE, and adenosine deaminase (that only binds one metal) Holm and Sander (1997) have recently identified an even larger set of enzymes that are predicted to have similar active site architectures. Indeed, a characteristic sequence signature of this superfamily includes the aspartate and the four histidine residues involved in metal binding within the active site. Many of the enzymes belonging to this superfamily are involved in nucleotide metabolism, including dihydroorotase, allantoinase, hydantoinases, and the AMP-, adenine, and cytosine deaminases. Also included in this superfamily are proteins involved in animal neuronal development and other enzymes such as imidazolonepropionase, arylalkylphosphatase, chlorohydrolase, and formylmethanofuran dehydrogenase. Note that some of these enzymes bind only one metal as in the case of adenosine deaminase. Thus far, no invariant lysine residues have been detected for other members

of this superfamily, suggesting that urease and PTE are unique in their employment of a carbamylated lysine residue as a bridging ligand.

K. MODIFICATIONS TO CARBAMYLATED LYSINE

The carbamylated lysine residue that serves to bridge the binuclear metal center is unusual. It is not clear why this function could not have been performed by a carboxylate side chain of either glutamate or aspartate. Perhaps this post-translational modification actively participates in the catalytic function of the active site or serves as a regulatory control mechanism for the assembly of the binuclear metal center. Hong et al. (1995) demonstrated that elevated levels of bicarbonate enhanced the rate of formation of the binuclear metal center when the apo-enzyme was mixed with divalent cations. For example, full reconstitution of the metal center in the absence of added bicarbonate is typically observed in 3 hours at room temperature. Preincubation with 100 mM bicarbonate prior to reconstitution with Cd^{2+} enhanced the rate of reactivation by a factor of about six. When the bridging lysine residue is mutated to either methionine (K169M) or alanine (K169A) the catalytic activity is drastically reduced. However, a significant fraction of the wild-type activity can be restored upon the addition of low molecular weight carboxylic acids. The activity of K169A was enhanced 25-fold in the presence of 100 mM propionic acid. Similarly, the activity of K169M was enhanced five-fold in the presence of 100 mM acetic acid (Kuo et al., 1997). The rescue of catalytic activity by the low molecular weight carboxylic acids demonstrate that the carbamate functional group is not absolutely required for the proper functioning of the binuclear metal center. It appears that these carboxylates can substitute for the bridging carbamate as shown in Scheme 3.



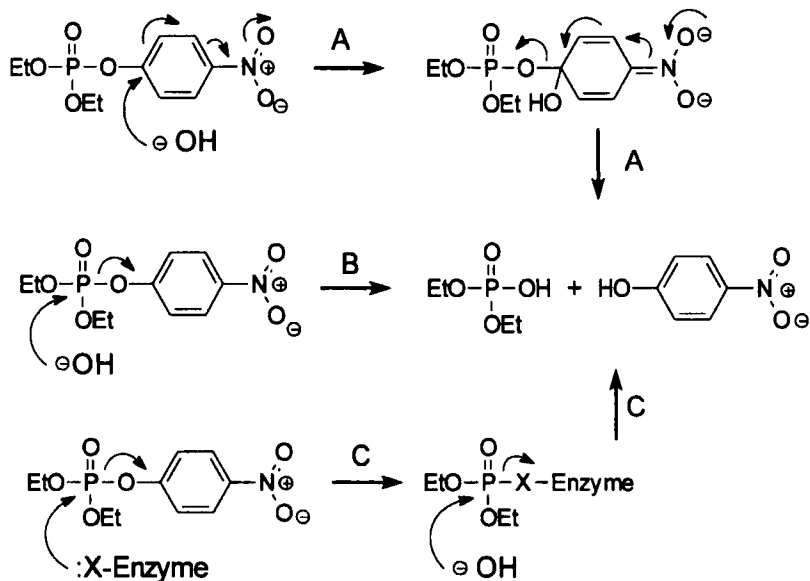
Scheme 3

Although the binuclear metal center in PTE is very similar to the one found in urease there are some notable differences. For example, the binuclear Ni^{2+} center in urease cannot be fully reassembled *in vitro* (Park and Hausinger, 1995). In fact, there appears to be a collection of accessory proteins that participate in the *in vivo* assembly of the binuclear metal center in urease.

III. Mechanism of Action

A. STEREOCHEMISTRY AT PHOSPHORUS CENTER

The general mechanism for the enzymatic hydrolysis of paraoxon can be viewed as proceeding by one of three possible routes (see Scheme 4). In mechanism A there is a nucleophilic attack at C-1 of the aromatic ring. This mechanism may appear to be highly unlikely but when these experiments were initiated the broad substrate specificity was not known for PTE. Moreover, removal of the electron withdrawing $-\text{NO}_2$ substituent diminished the



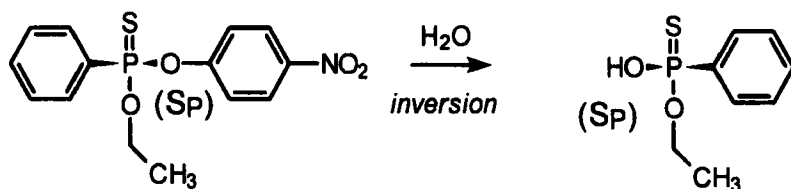
Scheme 4

overall reactivity by over five orders of magnitude. The intermediate or transition state in this particular mechanism could be stabilized by the resonance capability of the nitro group at C-4 of paraoxon. Subsequent C–O bond cleavage would yield the two products.

The second and third mechanisms can be described as variants of an S_N2 -like process that differ by the presence of a covalent enzyme-product intermediate. The second mechanism (**B**) involves a single displacement reaction at the phosphorus center. In this mechanism hydroxide, or an activated water molecule, attacks the phosphorus center yielding diethylphosphate and 4-nitrophenol in a single step. In the third mechanism (**C**) there are two in-line displacement reactions at the phosphorus center. The first would occur by a nucleophilic attack at the phosphorus atom by a side chain of a protein residue. This step would be followed by expulsion of 4-nitrophenol to produce the covalent enzyme product complex. Direct nucleophilic attack by water at the phosphorus would then yield diethylphosphate and regenerate free enzyme.

Two rather simple experiments were conducted that were able to differentiate among these three reaction mechanisms. When the reaction was conducted in oxygen-18 water, the heavy isotope was found exclusively in the diethylphosphate, proving that the bond cleavage occurred between the oxygen and phosphorus (Lewis et al., 1988). This result eliminated mechanism **A** from further consideration. In order to distinguish between mechanisms **B** and **C** the stereochemical course of the reaction at phosphorus was determined. If mechanism **C** was operable, then the reaction would proceed with net *retention* of configuration since each of the two steps in this mechanism would proceed with inversion of configuration. Since mechanism **B** has but a single step, the stereochemical course of the reaction would proceed with *inversion* of configuration.

Since neither the substrate nor product of paraoxon hydrolysis is chiral, this substrate cannot be utilized for this endeavor. Fortunately the substrate specificity was found to be promiscuous enough such that the S_p -isomer of the insecticide ethyl-p-nitrophenyl phenylphosphonothiate (EPN) was a good substrate for PTE. When the S_p -isomer of EPN is hydrolyzed by the enzyme, the product, ethyl phenylphosphonothioic acid, was found to have the S_p -configuration. Comparison of the relative stereochemistry of the substrate and product clearly indicated that the overall reaction proceeded with net *inversion* of configuration. Therefore PTE operates via mechanism **B** with a direct attack of an activated water molecule at the phosphorus center (Lewis et al., 1988). See Scheme 5.

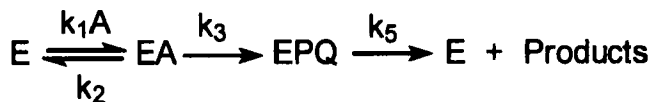


Scheme 5

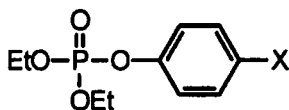
B. DETERMINATION OF RATE-LIMITING STEPS

The minimal reaction mechanism that can be written for PTE is presented in Scheme 6. In this scheme there is the simple binding of the triester to form the Michaelis complex (EA), the phosphorus-oxygen bond is cleaved to generate the enzyme-product complex (EPQ), and finally the products dissociate to regenerate the free enzyme for another round of catalysis. The reaction mechanism thus consists of a reversible *association* step, followed by an irreversible *chemical* event, and then the final *dissociation* of the reaction products. The relative magnitude for these three consecutive events was ascertained by a Brønsted analysis of the reaction. The objective of these experiments was to systematically alter the inherent chemical strength of the P–O bond to be cleaved. In the reaction catalyzed by PTE this objective was achieved through the utilization of leaving-group phenols having a range of pK_a values.

Caldwell et al. (1991a) reported the preparation of organophosphate triesters having the general structure shown in Scheme 7. The range of pK_a values spanned from 4.0–10.0. A plot of pK_a of the phenol versus k_{cat} is presented in Figure 15 (a plot of k_{cat}/K_m versus pK_a is similar). The change in the kinetic parameters does not appear to be the result of steric complications and thus the results can be interpreted based only on alterations in the step that involves the cleavage of the phosphorus-oxygen bond. Given this assumption, it is clear that there is a major change in the rate-limiting step as the pK_a of the leaving group phenol increases from 4 to 10.



Scheme 6



Scheme 7

For the kinetic model that appears in Scheme 6, the relationships for k_{cat} and k_{cat}/K_m are shown in equations 1 and 2.

$$k_{\text{cat}} = k_3 k_5 / (k_3 + k_5) \quad (1)$$

$$k_{\text{cat}} / K_m = k_1 k_3 / (k_2 + k_3) \quad (2)$$

The value of k_3 will vary according to the magnitude of the $\text{p}K_a$ of the leaving group phenol as shown in Equation 3 (Jencks and Carriuolo, 1961)

$$\log k_3 = (\beta \text{p}K_a) + C \quad (3)$$

These equations predict that as the chemical step, k_3 , becomes very fast, the maximum value for k_{cat} will be limited by the step for product release, k_5 . Conversely, the relative rates of slow substrates will be inversely proportional to the $\text{p}K_a$ of the leaving group phenol. Similarly, the limiting values for k_{cat}/K_m will approach k_1 as the $\text{p}K_a$ of the phenol becomes small. A fit of the data that appears in Figure 15 to a combination of equations 1 through 3 provides values of k_1 , k_2 , and k_3 of $4.1 \times 10^7 \text{ M}^{-1} \text{ s}^{-1}$, 2600 s^{-1} , and 2200 s^{-1} , respectively (Caldwell et al., 1991a). The value of β is -1.8 . There is clearly a change in rate-limiting step from product dissociation to bond cleavage as the $\text{p}K_a$ of the phenol increases.

The kinetic analysis of this mechanism yields a rather large β value of -1.8 compared to the values of -1.0 and -0.44 that have been observed for the chemical hydrolysis using water and hydroxide, respectively, as nucleophiles (Khan and Kirby, 1970). Therefore, for the enzymatic reaction, there is a higher sensitivity of the leaving group to the overall rate of hydrolysis. This result is consistent with a significant amount of charge transferred to the phenol in the transition state structure and thus implies that the P-O bond is very nearly completely broken. The observed difference between the β value for chemical and enzymatic hydrolysis may be attributed the hydrophobic environment at the active site.

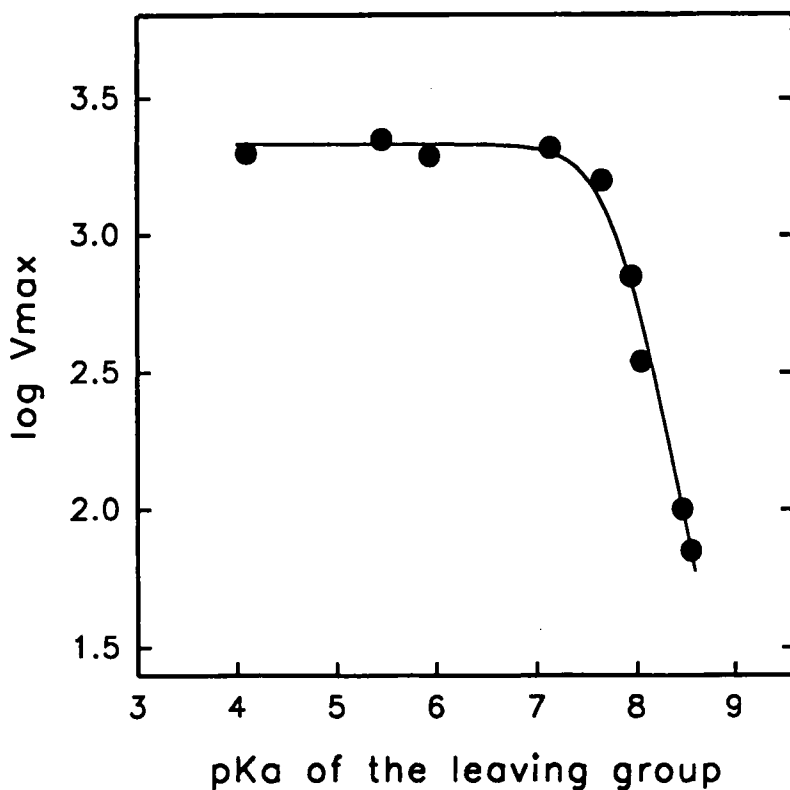


Figure 15. Brønsted plot for the enzymatic hydrolysis of a series of compounds with variable leaving groups.

C. EFFECTS OF SOLVENT VISCOSITY

Alterations in solvent viscosity have also been utilized to determine the relative magnitude of the rate constants presented in Scheme 6. Kirsch demonstrated that alterations in solvent viscosity alter those rate constants for processes that involve either the association or dissociation of enzyme-ligand complexes (Brouwer and Kirsch, 1982). The steps that involve the actual bond making or breaking within the active site are not affected. Thus, in Scheme 6, the rate constants k_1 , k_2 , and k_3 would be susceptible to changes in solvent viscosity while k_4 would not. The solvent viscosity experiments thus offered a nice complement to the previously described Brønsted analysis where these constants were held constant while k_3 was manipulated by changes in the pK_a

of the leaving group phenol. The effect on the kinetic parameter k_{cat}/K_m with changes in solvent viscosity conforms to Equation 4 (Caldwell et al., 1991a).

$$(k_{\text{cat}}/K_m)_0 / (k_{\text{cat}}/K_m) = (k_3\eta_{\text{rel}} + k_2) / (k_2 + k_3) \quad (4)$$

Equation 4 predicts a linear relationship between the relative second-order rate constant, $(k_{\text{cat}}/K_m)_0 / (k_{\text{cat}}/K_m)$ and the relative viscosity. The slope of this line provides a measure of the sensitivity of k_{cat}/K_m to changes in viscosity. From Equation 4, the slope is defined by the relationship shown in Equation 5.

$$(k_{\text{cat}}/K_m)_\eta = k_3 / (k_2 + k_3) \quad (5)$$

Therefore, the value of $(k_{\text{cat}}/K_m)_\eta$ can vary from 0 to 1 depending on the relative magnitude of the rate constants k_2 and k_3 . As k_3 becomes infinitely large, $(k_{\text{cat}}/K_m)_\eta$ approaches 1, and as k_3 becomes very small, $(k_{\text{cat}}/K_m)_\eta$ approaches 0. Shown in Figure 16 is the relationship between the $\text{p}K_a$ of the

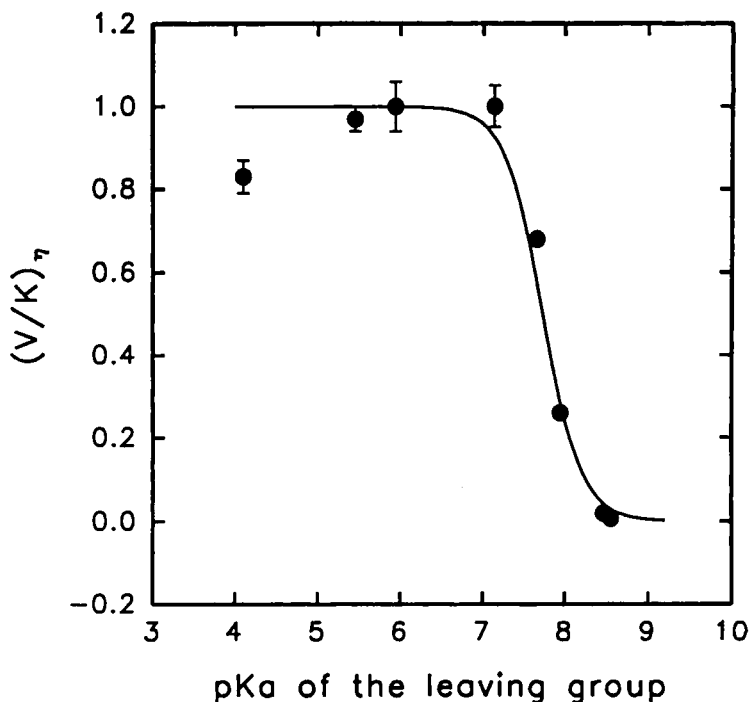


Figure 16. The change in the effect of solvent viscosity on the V/K values as a function of the $\text{p}K_a$ of the leaving group. The Zn/Zn-PTE was utilized for this experiment.

leaving group and $(k_{\text{cat}} / K_{\text{m}})_{\eta}$. Indeed, those substrates with leaving groups whose $\text{p}K_{\text{a}}$ values are <7 are limited by physical diffusion and $(k_{\text{cat}} / K_{\text{m}})_{\eta}$ approaches a value of unity. In contrast, the substrates with leaving group $\text{p}K_{\text{a}} >7$ are limited by the chemical step k_3 and $(k_{\text{cat}} / K_{\text{m}})_{\eta}$ approaches a value of 0. The solid line shown in Figure 16 represents a fit to equations 3 and 4 where $k_2 = 2150 \text{ s}^{-1}$, $\beta = -1.84$, and $C = 17.7$. The excellent fit of the viscosity data to the predicted values, based on the rate constants obtained from the Brønsted plot analysis, provides strong experimental support for this kinetic analysis.

D. pH-RATE PROFILES

The utilization of pH-rate profiles can, in certain circumstances, provide information critical to a fuller understanding of the reaction mechanism. Since the substrates hydrolyzed by PTE do not ionize between pH 4 and 10, all of the ionizations observed in such analyses must originate with the protein. Shown in Figure 2 is the pH-rate profile for the hydrolysis of paraoxon by the Zn/Zn-substituted enzyme. Since the catalytic activity does not diminish at high pH, there does not appear to be an enzyme functional group within the active site that offers general acid catalytic assistance to the leaving group. This assertion is supported by the lack of proton-donating residues in the active site from the X-ray crystallographic structure. Also, the extreme value of the Brønsted constant, β , argues against any suppression of the incipient negative charge via proton transfer.

The origin of the ionization that appears at pH ~ 6 is still unclear. Originally, this ionization was proposed to originate with the protonation of a histidine residue (Dumas and Raushel, 1990b). The histidine residue was postulated to serve as a general base in the abstraction of a proton from the hydrolytic water molecule. The effects of temperature and organic solvents were consistent with this notion. However, in view of the X-ray crystal structure the loss of activity at low pH may arise from the protonation of the bridging hydroxide between the two divalent cations. The variation of the kinetic $\text{p}K_{\text{a}}$ values upon alteration of the divalent cation itself is supportive of this proposal. When the active site is substituted with Zn^{2+} , Co^{2+} , Ni^{2+} , Mn^{2+} , and Cd^{2+} , the kinetic $\text{p}K_{\text{a}}$ values are 5.8, 6.5, 7.4, 7.0, and 8.1, respectively (Omburo et al., 1992). However, the loss of activity may occur indirectly through protonation of one of the four histidine residues that coordinate the two divalent cations within the active site. The nature the divalent cation may indeed perturb the ionization properties of the direct metal-ligand residues.

E. THE ROLE OF BINUCLEAR METAL CENTER

There are potentially three roles the binuclear metal center may play in the enzymatic hydrolysis of organophosphates. The metals may decrease the pK_a of the bound water molecule and increase the nucleophilic character of the attacking hydroxide. The metal ions can increase the polarization of the P=O bond, and thereby accelerate the approach of an attacking hydroxyl ion by increasing the electrophilic character of the phosphorus center. The metal ions may also neutralize the development of negative charge on the leaving group.

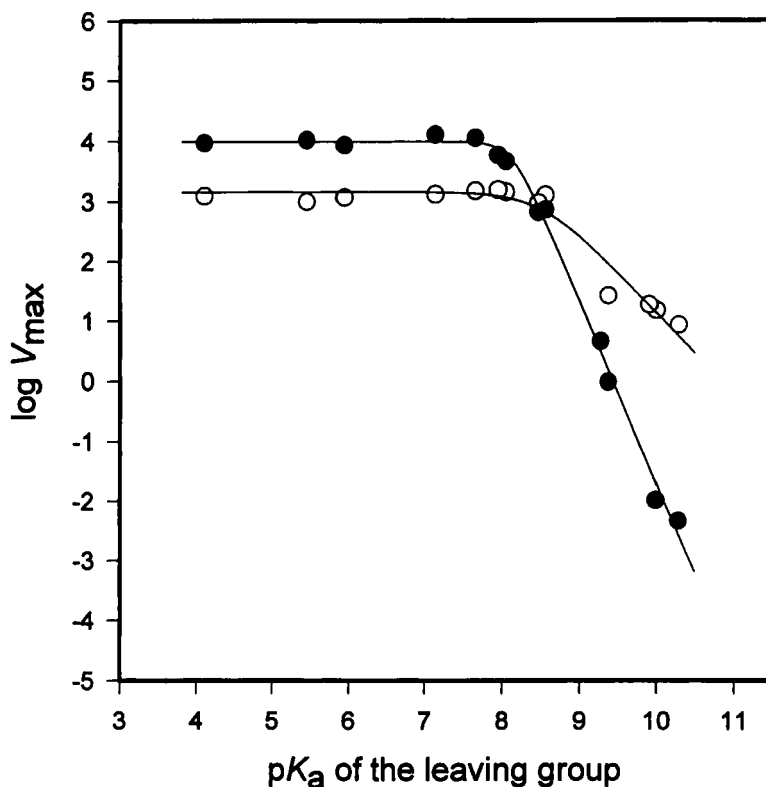
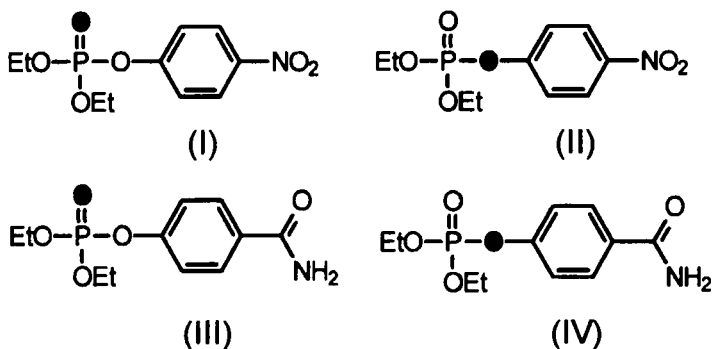


Figure 17. Brønsted plots for the dependence of $\log V_{max}$ on the pK_a of the leaving group. *Filled circles* are for a series of organophosphate triesters with leaving group phenols of variable pK_a values. *Open circles* are for a series of organothiophosphate triesters with leaving group phenols of variable pK_a values. The Cd/Cd-PTE was utilized for this experiment.

The direct interaction with the P=O of the substrate was probed by conducting Brønsted-type analyses with different metal-substituted variants of PTE and using a series of phosphate and thiophosphate organophosphate triesters. Shown in Figure 17 is the Brønsted plot for the hydrolysis of phosphate and thiophosphate triesters by Zn/Zn-PTE. Both plots are clearly nonlinear, representative of the change in rate-limiting step as discussed earlier (Caldwell et al., 1991a). It should be stated here that the hydrolysis of organophosphates by OH⁻ is about 20 times faster than the hydrolysis of the corresponding organothiophosphates (Hong and Raushel, 1996). When the rate-limiting step is dominated by something other than P-O bond cleavage (pK_a values of the leaving group phenols less than ~7) the organophosphate compounds are enzymatically hydrolyzed about one order of magnitude faster than the thiophosphates. For k_{cat} this likely means that the release of diethylthiophosphate is slower than the release of diethylphosphate from the enzyme-product complex. However, when substrates are utilized that are clearly limited by the rate of P-O bond cleavage, the thiophosphate analogs are more reactive than the phosphate series. Thus, there is a crossover in the relative magnitude of the kinetic constants. This observation supports the proposal that one or both of the metal ions in the binuclear metal center directly coordinates the phosphoryl group by polarization of the P=O (or P=S) bond. It has previously been demonstrated that the Cu²⁺-catalyzed hydrolysis of thiophosphotriesters is much more effective than with the corresponding oxygen analogs (Ketelaar et al., 1956). The faster rate of hydrolysis of the thiophosphate analogs can be explained by the direct coordination of one or both metal ions with the sulfur or oxygen atom of the substrates.

F. HEAVY ATOM ISOTOPE EFFECTS

Oxygen-18 isotope effects have been utilized to probe the transition state structure for the enzymatic and base-catalyzed hydrolysis of organophosphate triesters (Caldwell et al., 1991b, 1991c). The secondary and primary oxygen-18 isotope effects have been measured for PTE using the labeled substrate presented in Scheme 8. The nonbridge, or phosphoryl oxygen, serves as a reporter for the change in bond order in the transition state between this oxygen and the phosphorus core. This provides an indication of the degree of charge delocalization at this site upon attack by the incoming nucleophile. In a fully associative mechanism the attack of the nucleophile leads to a pentavalent phosphorane intermediate followed by the collapse of



Scheme 8

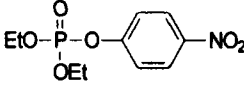
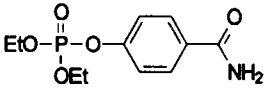
this structure to products. At the other extreme, the formation of an intermediate is not absolutely required with a direct-displacement mechanism and a single S_N2 -like transition state.

In a hybrid mechanism there is simultaneous, but not necessarily synchronous, decrease in bonding to both the phosphoryl oxygen and the leaving group upon the addition of the nucleophile. The relative magnitude of the bond order changes in the transition state at these two atoms is variable and dependent of the nucleophilic character of the attacking ligand and the ability of the leaving group to depart. The magnitude of the primary oxygen-18 effect will depend on the extent of bond cleavage to the leaving group while the secondary oxygen-18 isotope effect will be determined by the change in the bond order to the phosphoryl group.

Two sets of oxygen-18 labeled substrates have been tested with PTE. Paraoxon (**I** and **II**) is a relatively fast substrate for PTE and the kinetic constants k_{cat} and k_{cat}/K_m are limited primarily by diffusional steps rather than bond breaking steps while the other compound (**III** and **IV**) is a relatively poor substrate where the kinetic constants are dominated by bond breaking events. The primary and secondary isotope effects are listed for each of the compounds in Table 2.

The observed primary and secondary isotope effects exhibited by paraoxon are both quite small. This reflects to a significant extent that the chemical step is not rate-limiting. This is not, however, true for the slower substrate where the bond-breaking event is expected to be nearly fully rate-limiting. The extent of phosphorus-phenolic oxygen bond cleavage in the transition state can be estimated from the relative size of the intrinsic

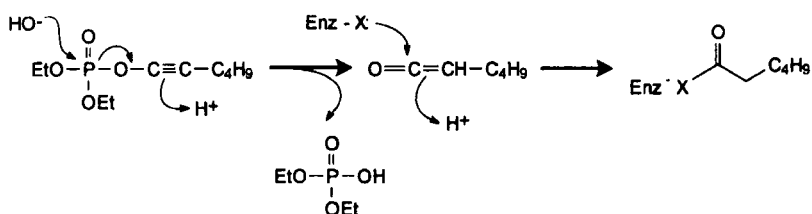
TABLE 2
Primary and Secondary Oxygen-18 Isotope Effects

Compound	$^{16}k/^{18}k$	$^{16}k/^{18}k$
	Primary	Secondary
	1.0020	1.0021
	1.036	1.0181

^{18}O -isotope effect. However, the maximum size of the ^{18}O -isotope effect for phosphotriester hydrolysis is unknown. However, the ^{18}O equilibrium isotope effect for the deprotonation of water and phenol has been estimated to be 1.039 (Rosenberg, 1977). The observed enzymatic effect is very close to this value and thus it appears that the P–O bond is nearly fully broken in the transition state. The secondary ^{18}O -isotope effect of 1.018 suggests that the bond order has changed from 2 to approximately 1.5. Taken together the isotope effects suggest that the reaction proceeds through an associative-type mechanism without any direct evidence for the formation of a phosphorane intermediate. The transition state structure is very product-like.

G. MECHANISM-BASED INHIBITORS

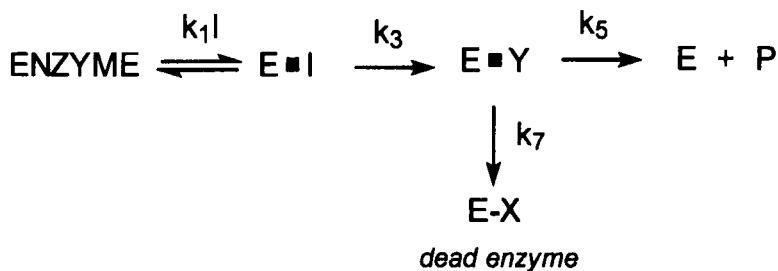
The bacterial PTE was among the first enzymes that catalyze a hydrolytic reaction at a phosphorus center to be inactivated by suicide substrates. The Stang laboratory synthesized a series of alkynyl phosphate esters (Stang et al., 1986). These compounds were constructed with the anticipation that cleavage of the phosphorus–oxygen bond would generate a highly reactive ketene intermediate as illustrated in Scheme 9. The electrophilic carbon center of the ketene intermediate could be subjected to attack by an adjacent nucleophile. Indeed, incubation of PTE with diethyl 1-hexynyl phosphate completely inactivated the enzyme in less than 2 minutes. The catalytic activity could not be recovered upon dialysis (Blankenship et al., 1991).



Scheme 9

The efficiency of enzyme inactivation was determined by incubation of a fixed enzyme concentration with variable concentrations of inhibitor. When the fraction of the original enzyme activity was plotted versus the initial ratio of inhibitor to enzyme the intercept on the horizontal axis is 1200. Therefore, approximately 1200 inhibitor molecules are enzymatically hydrolyzed for every enzyme molecule inactivated. The data have been analyzed according to the scheme presented in Scheme 10. In this scheme, **I** is the alkynyl phosphate ester, **Y** is the ketene intermediate, **E-X** is the inactivated enzyme, and **P** is a carboxylic acid after the ketene has reacted with water. The partitioning experiment described indicates that the ratio of k_5/k_7 is approximately 1200.

The inactivation reaction rate was determined using a stopped-flow device. At saturating inhibitor the rate constant for enzyme inactivation was 0.33 s^{-1} . The rate expression for the inactivation of PTE is shown in Equation 6. Since $k_5 \gg k_7$, the minimum value of the rate constant (k_7) for the reaction of the putative ketene intermediates is 0.33 s^{-1} . Thus, the minimum value of the rate constants for P-O bond cleavage and product release (k_3 and k_5) is



Scheme 10

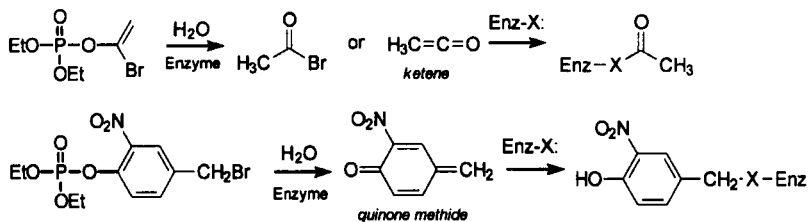
410 s⁻¹. These values compare quite favorably with the hydrolysis of paraoxon under similar conditions (2100 s⁻¹).

$$k_{in} = (k_3 k_7) / (k_3 + k_5 + k_7) \quad (6)$$

The identity of the residue within the active site that reacts with the putative ketene intermediate was initially probed with a radiolabeled alkynyl phosphate ester (Banzon et al., 1995a). After inactivation of enzyme activity, the stoichiometry of the labeled adduct to protein was 1:1 and the protein could be reactivated within 1.5 h at pH 10.0 (the labeling is conducted at pH 7.0). After the protein was inactivated there was an increase in absorbance at 245 nm ($\epsilon = 4400 \text{ M}^{-1} \text{ cm}^{-1}$). The change in UV absorbance and the reactivation kinetic studies ruled out all other amino acids except for the side chain of histidine.

The identity of the histidine residue that is critical for the maintenance of catalytic activity was probed using the seven histidine to asparagine mutants described earlier (Kuo and Raushel, 1994). Of the seven histidine to asparagine mutants only the H254N mutant was no longer susceptible to inactivation by either alkynyl phosphate esters or the histidine specific reaction, DEPC (Banzon et al., 1995b). The crystal structure of PTE shows that this residue is indeed within the active site but it is not a direct ligand to either of the two metal ions.

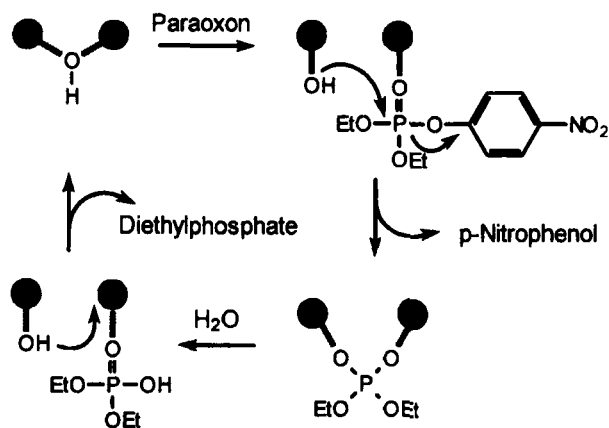
Additional ligands have also been designed as potential mechanism-based inactivators and inhibitors of PTE (Hong and Raushel, 1997; Hong et al., 1997). 1-Bromo vinyl- and 4-(bromomethyl)-2-nitro phenyl diethylphosphate (Stowell and Widlanski, 1994; Stowell et al., 1995) were found to be effective inactivators of the bacterial phosphotriesterase. The postulated reaction mechanisms are presented in Scheme 11.



Scheme 11

H. MECHANISM OF ACTION

The chemical probes of the reaction catalyzed by PTE enable a working model of the reaction mechanism to be formulated. The current model is limited by experimental constraints and certain details of the mechanism have not been settled. The working model for this reaction mechanism is illustrated in Scheme 12. The focal point of the model is the binuclear metal center. In order to facilitate this reaction the enzyme must accomplish three objectives. First, the hydrolytic water molecule must be activated for nucleophilic attack toward the phosphorus center of the substrate. The X-ray structure of PTE clearly shows that a solvent molecule bridges the two metal ions within the binuclear metal center. The coordination of the water molecule to the metal center would be expected to reduce the pK_a of the water and thus increase the local hydroxide concentration. There does not appear to be any basic residues within the active site that could serve to assist in the proton removal from any other solvent molecule. Second, the phosphorus center must be made more electrophilic. This can be achieved by coordination of the phosphoryl oxygen to one or both of the metal ions within the cluster. The ligation of the phosphoryl oxygen would polarize this bond and thus reduce the electron density at the phosphorus core. The variation in the β -values from the Brønsted experiments and the crossover in reactivity for the phosphate and thiophosphate substrates demonstrate that metal-substrate interactions are critical for efficient catalytic activity of



Scheme 12

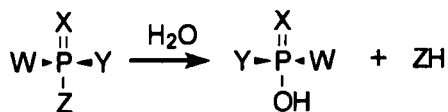
PTE. Third, the enzyme could activate the leaving group. The activation of the leaving group can potentially be accomplished by general acid catalysis using an appropriately placed residue or, alternatively, by Lewis acid catalysis. However, neither of these effects has thus far been demonstrated for PTE. The best substrates (such as those with *p*-nitrophenolate leaving groups) do not require any significant assistance and there does not appear to be any side chains positioned in the three-dimensional structure of PTE that could serve this function.

The proposed reaction mechanism is initiated by the binding of the substrate to the binuclear metal center. One of the interactions from the metal to the bridging solvent molecule is broken and replaced by ligation to the phosphoryl oxygen of the substrate. Nucleophilic attack is initiated by the bound hydroxide toward the phosphorus center. For substrates such as paraoxon the transition-state is developed quite late. Part of the incoming negative charge is dispersed to the phosphoryl oxygen (via interaction with the metal ion) while the rest is dispersed through the aromatic ring system of the departing phenolate. After the phenolate has departed the product complex would now bridge the two metal ions. However, structural evidence for this type of complex has not been obtained. In the final step, the product would be displaced by an incoming solvent molecule prior to the next round of catalysis.

There are a number of issues with regard to this mechanism that remain unresolved. The pK_a value of the bridging solvent molecule is unknown. It has been assumed in the past that it is the pK_a of this group that is reflected in the pK_a values determined by variation of the kinetic parameters with pH. Perhaps this issue can be settled using NMR or EPR spectroscopic methods. It is also unclear if the two metal ions within the binuclear metal center have distinct functions or whether they operate as a true tandem pair. The catalytic properties of the unique Cd/Zn-hybrid would argue for separate functions for each of the two metals. Resolution of this issue may be obtained when the specific binding sites are determined for the Zn^{2+} and Cd^{2+} in the hybrid cluster of PTE by X-ray crystallography.

IV. Substrate Specificity

The substrate specificity for PTE is actually quite broad. For the prototypic reaction illustrated in Scheme 13 the substituent X can either be oxygen or sulfur (Donarski et al., 1989). In a limited investigation it was shown that the thiophosphate esters are hydrolyzed faster than the corresponding phosphate esters when the rate-limiting step was actual bond cleavage



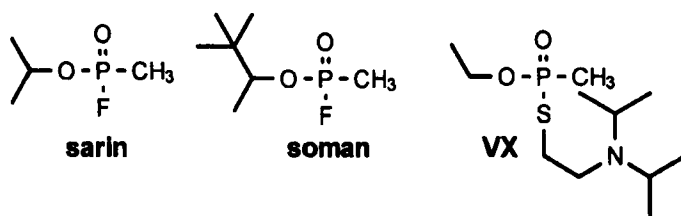
Scheme 13

(Hong and Raushel, 1996). However, when the rate-limiting step is product release or an associated conformational step, then the turnover of the phosphate derivative was faster than thiophosphate analog.

A variety of substituents have been shown to be viable when attached to the non-leaving group positions (**W** and **Y**). High rates of turnover have been measured for CH_3 -, CH_3O -, $\text{CH}_3\text{CH}_2\text{O}$ -, $(\text{CH}_3)_2\text{CHO}$ -, C_6H_5 -, $\text{C}_6\text{H}_5\text{O}$ -, $n\text{C}_4\text{H}_9\text{O}$ -, $n\text{C}_3\text{H}_7\text{O}$ -, among others (Donarski et al., 1989; Hong and Raushel, 1999). Fully esterified phosphonates are hydrolyzed as well as organophosphate triesters.

The enzyme exhibits a significant amount of stereoselectivity toward the hydrolysis of chiral organophosphates. The first demonstration of this was reported for the hydrolysis of a racemic mixture of EPN. The enzyme greatly prefers the S_p -isomer over the R_p -isomer (Lewis et al., 1988). More recently, an extensive analysis of the substrate preferences for the chiral forms of a series of organophosphate triesters was initiated. Nearly all possible combinations of the various substituents were analyzed as substrates when **W** and **Y** were changed to CH_3 -, CH_3CH_2 -, $(\text{CH}_3)_2\text{CH}$ -, or C_6H_5 -. In every case examined, the S_p -isomer was hydrolyzed significantly faster than the R_p -isomer. The single exception was with the two smallest substituents, methyl and ethyl. These small alkyl substituents could not be distinguished from one another.

The substituents that can participate as leaving groups are more restricted. A wide range of substituted phenols are substrates but the turnover numbers are very dependent on the $\text{p}K_a$ of the phenol (see Brønsted plots). Since the β -value approaches a value of nearly 2, the k_{cat} for substrates with phenol as a leaving group ($\text{p}K_a \sim 10$) are reduced by a factor of nearly a million relative to those with *p*-nitrophenol as the leaving group. However, the leaving groups are not restricted to phenols. Fluoride and alkylthiols are also tolerated but the turnover numbers are quite slow (Dumas et al., 1989b, 1989c; Chae et al., 1994). The hydrolysis of extremely toxic substances such as sarin, soman, and VX (Scheme 14) has suggested that this enzyme could be utilized to detect and detoxify a variety of military-type organophosphate nerve agents.



Scheme 14

A host of compounds are not hydrolyzed as a significant rate. No reaction was detected with *p*-nitrophenyl acetate and thus the enzyme will not hydrolyze simple carboxylate esters (Donarski et al., 1989). The enzyme will not hydrolyze sulfonate esters or phosphoramides. It was originally thought that organophosphate diesters were not hydrolyzed but it was later shown that diesters could be hydrolyzed but at a rate that was reduced by a factor of 10^5 (Shim et al., 1998).

A. ALTERATIONS TO SUBSTRATE SPECIFICITY

The high catalytic turnover of the wild-type enzyme and the tolerance for modification to the substrate phosphorus core has prompted a number of efforts designed to enhance and expand the substrate specificity. For example, the wild-type enzyme has been shown to hydrolyze phosphorofluoridates such as diisopropyl fluorophosphate (DFP) with turnover numbers for the wild-type enzyme that were about 50 s^{-1} when the divalent cation was Zn^{2+} (Dumas et al., 1989b, 1989c). The rate could be enhanced by about an order of magnitude when the native Zn^{2+} was replaced with Co^{2+} (Watkins et al., 1997b). Finally, turnover numbers in excess of 3000 s^{-1} could be achieved when two residues within the substrate binding pocket were mutated (Watkins et al., 1997b). This came about when Phe-132 and Phe-136 were mutated to histidine residues. This substitution provided a more polar environment in the vicinity of the leaving group and also provided potential general acid substituents.

The ability to hydrolyze organophosphate diesters has also been subjected to mutagenesis. If one removes one of the ethyl groups from paraoxon the turnover number decreases by a factor of $\sim 100,000$. A significant fraction of the decrease in catalytic activity derives from the fact that organophosphate diesters are inherently less reactive than the corresponding triesters. An examination of the substrate-binding site reveals that the amino acids that con-

stitute the active site are largely hydrophobic and thus not very tolerant of the negative charge of potential diester substrates. Incremental enhancements to the rate of hydrolysis of diester substrates could be obtained by the introduction of cationic residues within the active site (Shim et al., 1998). Enhancement of diester hydrolysis could be obtained by the addition of alkyl amines to the reaction mixture. The amines are thought to enhance the rate of diester hydrolysis by filling the cavity that is left within the active site upon removal of one of the alkyl substituents from a triester substrate and neutralization of the negative charge. The most dramatic effect came about when diethylamine (2.0 M) was added. The V/K value changed from $1.6 \text{ M}^{-1} \text{ s}^{-1}$ to $260 \text{ M}^{-1} \text{ s}^{-1}$. The substrate specificity can also be manipulated. For example, the k_{cat} for demeton-S is increased by a factor of 12 when His-254 and His-257 are mutated to arginine and leucine respectively (diSoudi et al., 1999).

Summary

The bacterial PTE is able to catalyze the hydrolysis of a wide range of organophosphate nerve agents. The active site has been shown to consist of a unique binuclear metal center that has evolved to deliver hydroxide to the site of bond cleavage. The reaction rate for the hydrolysis of activated substrates such as paraoxon is limited by product release or an associated protein conformational change.

Acknowledgments

The work in the author's laboratory on the structure and mechanism of PTE has been supported in part by the NIH (GM33894, GM55513), Office of Naval Research, Robert Welch Foundation (A-840), and the Advanced Technology Program from the State of Texas.

References

- Antanaitis BC, Brown RD, Chasteen ND, Freeman JH, Koenig SH, Lilienthal HR, Peisach J, Brewer CF (1987): *Biochemistry* 26: 7932–7937.
- Banzon JA, Kuo JM, Fischer DR, Stang PJ, Raushel FM (1995a): *Biochemistry* 34: 743–749.
- Banzon JA, Kuo JM, Miles BW, Fischer DR, Stang PJ, Raushel FM (1995b): *Biochemistry* 34: 750–754.
- Beese LS, Steitz TA (1991); *EMBO J* 10: 25–33.
- Benning MM, Kuo JM, Raushel FM, Holden HM (1994): *Biochemistry* 33: 15001–15007.

- Benning MM, Kuo JM, Raushel FM, Holden HM (1995): *Biochemistry* 34: 7973–7978.
- Blankenship JN, Abu-Soud H, Francisco WA, Raushel FM, Fischer DR, Stang PJ (1991) *J Am Chem Soc* 113: 8561–8562.
- Brouwer AC, Kirsch JF (1982): *Biochemistry* 25: 1302–1307.
- Brown KA (1980): *Soil Biol Biochem* 12: 105–112.
- Buchbinder JL, Stephenson RC, Dresser MJ, Pitera JW, Scanlan TS, Fletterick RJ (1998): *Biochemistry* 37: 5096–5106.
- Caldwell SR, Newcomb JR, Schlecht KA, Raushel FM (1991a): *Biochemistry* 30: 7438–7444.
- Caldwell SR, Raushel FM, Weiss PM, Cleland WW (1991b): *Biochemistry* 30: 7444–7450.
- Caldwell SR, Raushel FM, Weiss PM, Cleland WW (1991c): *J Am Chem Soc* 113: 730–732.
- Chae MY, Omburo GA, Lindahl PA, Raushel FM (1993): *J Am Chem Soc* 115: 12173–12174.
- Chae MY, Postula JF, Raushel FM (1994): *Bioorg Med Chem Lett* 4: 1473–1478.
- Chae MY, Omburo GM, Lindahl PA, Raushel FM (1995): *Arch Biochem Biophys* 316: 765–772.
- diSoudi B, Grimsley JK, Lai K, Wild JR (1999): *Biochemistry* 38: 6534–6540.
- Donarski WJ, Dumas DP, Heitmeyer DP, Lewis VE, Raushel FM (1989): *Biochemistry*, 28: 4650–4655.
- Dumas DP, Caldwell SR, Wild JR, Raushel FM (1989a): *J Biol Chem* 264: 19659–19665.
- Dumas DP, Wild JR, Raushel FM (1989b): *Biotech Appl Biochem* 11: 235–243.
- Dumas DP, Durst HD, Landis WG, Raushel FM, Wild JR (1989c): *Arch Biochem Biophys* 277: 155–159.
- Dumas DP, Raushel FM (1990a): *Experientia* 46: 729–731.
- Dumas DP, Raushel FM (1990b): *J Biol Chem* 265: 21498–21503.
- Farber GK, Petsko GA (1990): *Trends Biochem Sci* 15: 228–234.
- Goldberg J, Huang H-B, Kwon Y-G, Greengard P, Nairn AC, Kuriyan J (1995): *Nature* 376: 745–753.
- Holm L, Sander C (1997): *Proteins: Structure Function, and Genetics* 28: 72–82.
- Hong S-B, Kuo JM, Mullins LS, Raushel FM (1995): *J Am Chem Soc* 117: 7580–7581.
- Hong S-B, Raushel FM (1996): *Biochemistry* 35: 10904–10912.
- Hong S-B, Mullins LS, Shim H, Raushel FM (1997): *Biochemistry* 36: 9022–9028.
- Hong S-B, Raushel FM (1997): *J Enzyme Inhibition* 12: 191–203.
- Hong S-B, Raushel FM (1999): *Biochemistry* 38: 1159–1165.
- Hough E, Hansen LK, Birknes B, Jynge K, Hansen S, Hordvik A, Little C, Dodson E, Derewenda Z (1989): *Nature* 338: 357–360.
- Jabri E, Carr MB, Hausinger RP, Karplus PA (1995): *Science* 268: 998–1004.
- Jencks WP, Carriuollo J (1961): *J Am Chem Soc* 83: 1743–1750.
- Kahn SS, Kirby AJ (1970): *J Chem Soc B* 1970: 1172–1182.
- Ketelaar JAA, Gersmann HR, Beck MM (1956): *Nature* 77: 1956–1957.
- Khangulov SV, Barynin VV, Antonyuk-Barynina SV (1990): *Biochim Biophys Acta* 1020: 25–33.

- Kim EE, Wyckoff HW (1991): *J Mol Biol* 218: 449–464.
- Kuo JM, Raushel FM (1994): *Biochemistry* 33: 4265–4272.
- Kuo JM, Chae MY, and Raushel FM (1997): *Biochemistry* 36: 1982–1988.
- Lai K, Dave KI, Wild JR (1994): *J Biol Chem* 269: 16579–16584.
- Lewis VE, Donarski WJ, Wild JR, Raushel FM (1988): *Biochemistry* 27: 1591–1597.
- McDaniel CS (1985): Ph.D. Dissertation Texas A&M University, College Station, Texas.
- Mulbry WW, Karns JS (1989): *J Bacteriol* 171: 6740–6746.
- Munneke DM (1976): *Appl Environ Microbiol* 32: 7–13.
- Omburo GA, Kuo JM, Mullins LS, Raushel FM (1992): *J Biol Chem* 267: 13278–13283.
- Omburo GA, Mullins LS, and Raushel FM (1993): *Biochemistry* 32: 9148–9155.
- Park I-S, Hausinger RP (1995): *Science* 267: 1156–1158.
- Pollack SJ, Atack JR, Knowles MR, McAllister G, Ragan CI, Baker R, Fletcher SR, Iversen LL, Broughton HB (1994): *Proc Natl Acad Sci USA* 91: 5766–5770.
- Poyner RR, Reed GH (1992): *Biochemistry* 31: 7166–7173.
- Reczykowski RS, Ash DE (1992): *J Am Chem Soc* 114: 10992–10994.
- Rosenberg S (1977): Ph.D. Dissertation, University of California, Berkeley.
- Rowland SS, Speedie MK, Pogell BM (1991): *Appl Environ Microbiol* 57: 440–444.
- Scanlan TS, Reid RC (1995): *Chem Biol* 2: 71–75.
- Serdar CM, Murdock DC, Rohde MF (1989): *Biotechnology* 7: 1151–1155.
- Shim H, Hong S-B, Raushel FM (1998): *J Biol Chem* 273: 17445–17450.
- Stang PJ, Boehshar M, Lin J (1986): *J Am Chem Soc* 108: 7832–7836.
- Stowell JK, Widlanski TS (1994): *J Am Chem Soc* 116: 789–790.
- Stowell JK, Widlanski TS, Kutateladze TG, Raines RT (1995): *J Org Chem* 60: 6930–6936.
- Sträter N, Lipscomb WN (1995): *Biochemistry*, 34: 9200–9210.
- Sträter N, Klabunde T, Tucker P, Witzel H, Krebs B (1995): *Science* 268: 1489–1492.
- Summers MF (1988): *Coord Chem Rev* 86: 43–134.
- Vanhooke JL, Benning MM, Raushel FM, Holden HM (1996): *Biochemistry* 35: 6020–6025.
- Volbeda A, Lahm A, Sakiyama F, Suck D (1991): *EMBO J* 10: 1607–1618.
- Watkins LM, Kuo JM, Chen-Goodspeed M, Raushel FM (1997a): *Proteins: Structure. Function, Genetics* 29: 553–561.
- Watkins LM, Mahoney HJ, McCulloch JK, Raushel FM (1997b): *J Biol Chem* 272: 25596–25601.
- Wilcox DE (1996): *Chem Rev* 96: 2435–2458.